Isotopic Spin $I=0$

$$z_0=\gamma\left[\frac{b_{11}+\gamma l_{22}\det b}{1+\gamma l_{22}b_{22}}\right],$$

$$\eta_0=\frac{b_{12}}{b_{11}+\gamma l_{22}\det b}.$$

Isotopic Spin $I=1$

$$z_1=\gamma\frac{b_{11}+\gamma l_{22}(b_{11}b_{22}-b_{12}b_{21})+\gamma l_{33}(b_{11}b_{33}-b_{13}b_{31})+\gamma^2 l_{22}l_{33}\det b}{1+\gamma[l_{22}b_{22}+l_{33}b_{33}+l_{22}l_{33}(b_{22}b_{33}-b_{23}b_{32})]},$$

$$\eta_1=[b_{12}-\gamma l_{33}(b_{13}b_{32}-b_{21}b_{33})]/\Delta,$$

where

$$\nu_1=[b_{13}-\gamma l_{22}(b_{12}b_{33}-b_{31}b_{22})]/\Delta,$$

$$\Delta=b_{11}+\gamma l_{22}(b_{11}b_{22}-b_{12}b_{22})+\gamma l_{33}(b_{11}b_{33}-b_{13}b_{31})+\gamma^2 l_{22}l_{33}\det b.$$

$K^- - p$ and $K^- - n$ Cross Sections in the Momentum Range 1–4 Bev/c

V. Cook, Bruce Cork, T. F. Hoang, D. Keefe, L. T. Kerth, W. A. Wenzel, and T. F. Zipf

Lawrence Radiation Laboratory, University of California, Berkeley, California

(Received February 27, 1961)

The energy dependence of the K^--nucleon total cross sections has been measured over the K^- momentum range 0.98–3.98 Bev/c. $K^- - n$ cross sections were obtained by deuterium-hydrogen subtraction, with a correction for screening effects. There is evidence for structure in the $T=0$ K^--nucleon state in the momentum range 0.98–2.0 Bev/c. This structure is absent in the $T=1$ state. In addition, a measurement was made at 1.95 Bev/c of the angular distribution of the $K^- - p$ elastic scattering at small angles. The forward-scattering amplitude obtained from the data gives a ratio of real part to imaginary part 0.5±0.2 at 0°. The corresponding ratio for π^- mesons at this momentum was found to be $0.4_{-0.4}^{+0.2}$.

Measurements of the $K^- - p$ "elastic" charge exchange gives a cross section which falls from about 10 mb at 1 Bev/c to at most a few mb at 4 Bev/c.

I. INTRODUCTION

SEVERAL measurements of the $K^- - p$ total cross section at different energies have been made previously by means of bubble chambers, counters, and nuclear emulsions.[1] These in general have rather large errors and are too widely spaced to allow much more than the general trend of the cross section with energy to be inferred. At energies less than a few hundred Mev, the data suggest a $1/v$ dependence, and the higher-energy points are consistent with a smoothly falling curve, the slope diminishing as the energy increases. The object of the experiment presented here was to determine to a precision of a few percent both the $K^- - p$ and $K^- - n$ total cross sections in the high-energy region ($p_K \geqslant 1$ Bev/c). The upper limit in momentum ($p_K = 4$ Bev/c) was the highest at which a convenient flux of K^- mesons could still be obtained at the Bevatron. In addition, the cross section for the charge-exchange

reaction

$$K^- + p \rightarrow \bar{K}^0 + n,$$
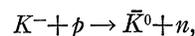
was measured at four different values of incident momentum. The angular distribution for small-angle $K^- - p$ scattering ($\theta_{\text{lab}} \lesssim 30$ deg), and the forward-scattering cross section, were measured at a single K^--meson momentum of 1.95 Bev/c.

II. THE K^- BEAM

A. Beam Layout

Figure 1 shows the arrangement of counters and magnets used to obtain a variable-energy K^--meson beam. The primary target was of stainless steel, $5\times\frac{1}{2}\times\frac{1}{4}$ in., placed in the magnet gap of the Bevatron. Negative particles, produced within about 5 deg to the direction of the circulating 6.2-Bev proton beam, entered the channel through a 0.020-in. aluminum window in the vacuum tank at the beginning of the west straight section. The first bending magnet M_1 was used to correct for variation in apparent target position with

---

[1] For a recent compilation of data and references see, for example, T. F. Kycia, L. T. Kerth, and R. G. Baender, Phys. Rev. **118**, 553 (1960).
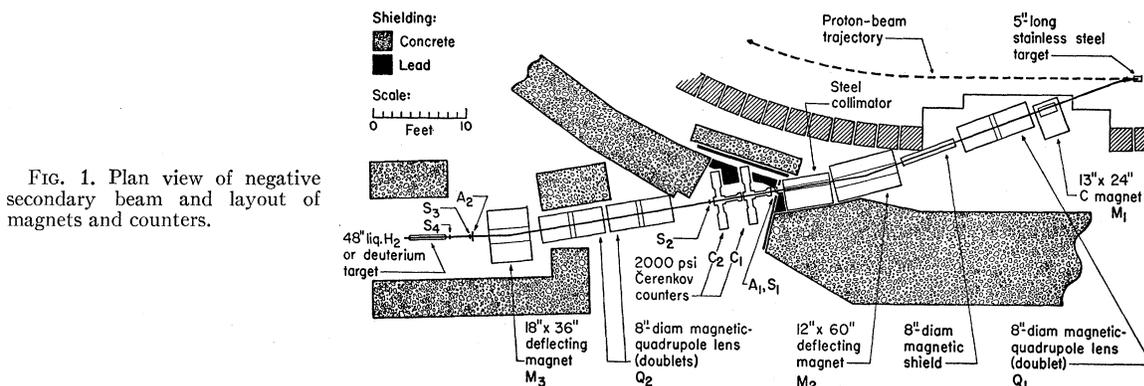
FIG. 1. Plan view of negative secondary beam and layout of magnets and counters.

selected momentum. The exact definition of operating momentum was by means of the two bending magnets M_2 and M_3, both of which were calibrated in advance by the floating-wire technique. The first quadrupole doublet Q_1 produced an image of the internal target between the beam scintillation counters S_1 and S_2.

The dimensions and location of S_1 and S_2 with respect to bending magnet M_1 determined the upper and lower limits of momentum selected; the full width of this interval varied between 6.8% and 10.5%, depending on the energy. This image of the target was in turn focused by the quadrupole lens triplet Q_2 at the transmission counter T behind the hydrogen target. The intervening bending magnet M_3 served to reject degraded particles and correct the dispersion of M_1. Polyethylene bags filled with helium were used in the collimator, magnet, and quadrupole lens apertures to reduce the effect of multiple Coulomb scattering.

The two gas Čerenkov counters C_1 and C_2, together with the two time-of-flight counter pairs S_1-S_3 and S_2-S_4, selected the K^- mesons in the beam and rejected π^- mesons, μ^- mesons, electrons, and antiprotons. C_1 and C_2 were placed together at the first image so that multiple Coulomb scattering in the high-pressure gas and aluminum end windows of the counters did not lead to any aberration in the final image, although it produced some loss in intensity.

The hydrogen target was 48 in. long and 6 in. in diameter, with 0.005-in. stainless steel walls and end windows, and could be filled with either hydrogen or deuterium.

B. Gas Čerenkov Counters C_1 and C_2: Selection of K Mesons

Selection of K mesons and rejection of other particles was made mainly by the two gas Čerenkov counters C_1 and C_2, which could be filled with gaseous methane to a maximum pressure of 2000 psi. Figure 2 shows a simplified cross-sectional view of one counter. The radiating volume of gas is approximately 24 in. long by 5 in. in diameter. A particle of velocity βc traveling parallel to the axis produces a cone of Čerenkov light of

half-angle θ, given by $\cos\theta = 1/n\beta$, where n is the refractive index of the gas. Some of this light strikes the two 45 deg mirrors directly, the rest after one reflection at the cylindrical reflector lining the inside of the barrel. After the light is deflected into the side arms of the counter, ring foci of angular radius θ are produced by the two Lucite lenses shown. If the angular radius of the ring focus is less than 6.7 deg, all light at the image is brought through a conical light pipe to a centrally located 2-in. RCA 6810A photomultiplier. If the angular radius exceeds 7.4 deg, however, no light strikes the central multiplier, but instead is brought via four flared light pipes to the photocathodes of four interconnected 2-in. RCA 6810A photomultipliers placed in a ring; two of these can be seen in the cross sectional view. The dichotomy in the range of θ selected by inner or outer photomultipliers is ensured by a narrow steel annular stop which also serves as a support for the quartz pressure window.

The Čerenkov counters were operated in either of two ways, mode A or B, depending upon whether the K-meson momentum was greater or less than 1.5 Bev/c. In mode A operation, the gas pressure was set so that for the momentum chosen a K meson produced Čerenkov
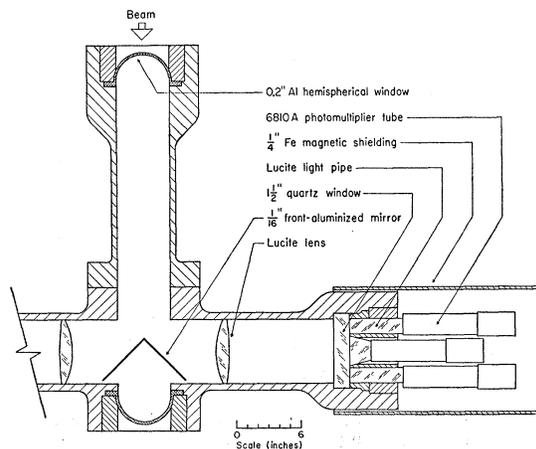
FIG. 2. Cross section of one of the methane Čerenkov counters.

radiation at an angle $\theta=6$ deg and would give a signal in the central photomultiplier in each arm. In the range of energies under investigation, π and μ mesons and electrons always produced Čerenkov light at a large enough angle to give a signal in the outer ring of photomultipliers. Thus, signals from the inner photomultipliers C_{inner} were used for positive identification of K mesons, and signals from the outer photomultipliers C_{outer} were used to reject, by anticoincidence, unwanted lighter particles. During the experiment the C_{inner} and C_{outer} signals from both arms of a counter were, respectively, connected in parallel. To minimize the accidental counting rate, coincidence-anticoincidence combinations of the two types $(C_{inner})_1+S_1+S_3-(C_{outer})_1$ and $(C_{inner})_2+S_2+S_4-(C_{outer})_2$ were formed, and the outputs from these two combinations finally put into coincidence. The time-of-flight system gave some discrimination against antiprotons, particularly at the low momenta.

Figure 3 shows a delay curve obtained when delay was varied between the Čerenkov counter outputs and two time-of-flight scintillators S_3 and S_4. When the counters are "on time," K mesons are counted (central peak) at a rate corresponding to about 0.1% of the π-meson rate. If the timing is off by a large amount, say 50 mμsec, then the K mesons selected at the Čerenkov counters are never counted in the downstream scintillators, and the steady background level of $K^-/M_2\approx 2$
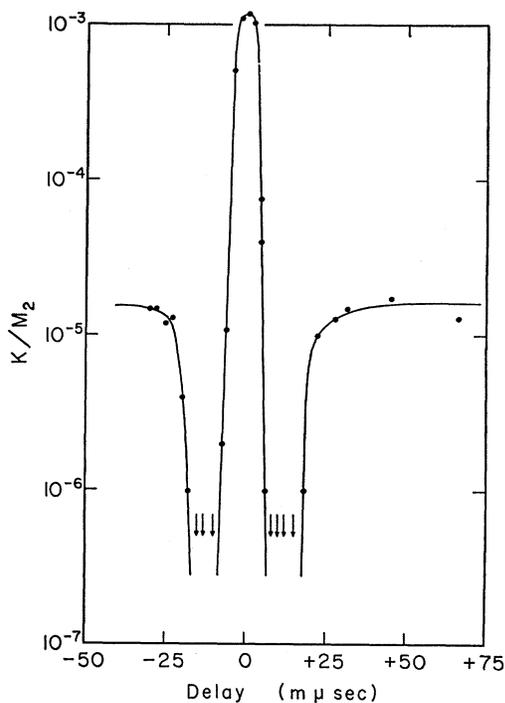
FIG. 3. Delay curve illustrating effectiveness of the anticoincidence circuit in reducing the accidental rate for particles arriving within ±20 mμsec of the passage of a K meson. The monitor M_2 measures the flux of particles in the beam channel.

$\times 10^{-5}$ is due to off-time light-meson accidentals. If, however, the delay is only about ±10–20 mμsec, then the anticoincidence pulse produced by the off-time particle results in a reduction of the accidental rate of some two orders of magnitude, at least. Thus, in measuring cross sections, for example, high resolution is not required for the transmission counter coincidence circuits, as the background accidental rate is negligible for times of ±20 mμsec about the arrival time of a K meson.

At each value of operating momentum, the rejection efficiency of the Čerenkov counters was checked and the best value of working pressure obtained by plotting the apparent K-meson counting rate as a function of the pressure in the counters. A typical pressure curve obtained for $p_K=2$ Bev/c is shown in Fig. 4 (mode A).

In the range of pressures 100–400 psi, the counting rate is very high and almost equal to that in the scintillators $S_1+S_2+S_3+S_4$, since the refractive index of the gas at these pressures is such that π and μ mesons produce Čerenkov light with $\theta<6.7$ deg, and so are counted by the inner photomultipliers. As the pressure is driven higher, the angle of the Čerenkov cone grows larger and light shifts to the outer ring (anticoincidence), resulting in a sharp falloff (approx 10^{-6}) in counting rate. Above about 700 psi the threshold for K mesons is crossed, and the K-counting rate reaches a maximum at about 1000 psi ($\theta_K\approx 6$ deg), and then falls off again at higher pressures as light due to K mesons is driven into the outer anticoincidence ring. At this momentum the shape of the curve shown indicates an operating pressure of 1030 psi and guarantees a K-meson beam with a contamination of less than one part in 10^3. Contamination at all momenta was also estimated to be less than 10^{-2}.
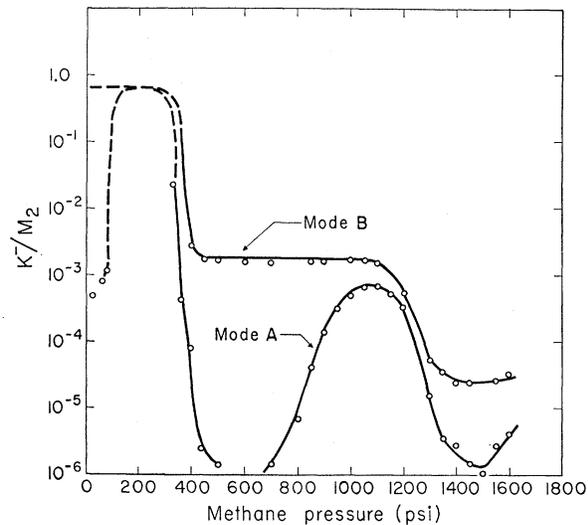
FIG. 4. Pressure curve for the Čerenkov counter-beam counter coincidence arrangement for $p_K=1.95$ Bev/c. M_2 refers to the counting rate of all particles coming down the channel. Mode A corresponds to coincidence-anticoincidence operation and mode B to anticoincidence operation only.

For momenta below 1.5 Bev/c, there were two disadvantages in mode A operation: The momentum bandwidth of the counters became narrower than that set by the geometry of the beam-defining scintillators, and the operating pressures became inconveniently large. Instead, then, mode B operation was used, in which the positive signal C_{inner} was not required and each counter was employed purely as an anticoincidence device. Mode B in Fig. 4 shows the type of pressure curve obtained under these circumstances. At low pressures no particles are rejected, but as the pressure is raised beyond about 400 psi, π and μ mesons begin to give C_{outer} signals, and a long plateau corresponding to the counting of K mesons and antiprotons extends up to about 1050 psi, beyond which only antiprotons can be counted. In operating on this plateau, no difficulty arises from the presence of the antiprotons; they can be eliminated by the time-of-flight system, since the flight-time difference between K^- and $\bar{p}$ exceeds 4 mμsec for $p \leqslant 1.5$ Bev/c. In mode B, the two counters were in fact operated at different pressures. In C_1, the pressure was set so that the light produced by π mesons of the correct momentum was focused centrally in the outer annulus; this pressure was usually about 700–800 psi. In C_2, in which the side arms of the counter were lined with a cylindrical reflector, the operating pressure was set very much higher (approx 1500–1700 psi), so that light from π mesons of the selected momentum ($\theta \approx 18$ deg) struck the anticoincidence photomultipliers only after reflection at the wall. But now π mesons of very much lower momentum could give anticoincidence pulses, provided they produced Čerenkov light with $\theta > 7.4$ deg. This arrangement allowed rejection of π mesons of the central momentum with maximum efficiency in C_1, and rejection of both degraded and undegraded π mesons in C_2.

C. Yield of K^- Mesons

During typical operation, the number of particles passing down the beam channel was between 1 and 4×10^5 per Bevatron pulse (about 1.5×10^{11} protons). At 2 or 3 Bev/c the number of K mesons counted in the system per pulse was about 600. At high momenta, the yield diminished rapidly because of the decreased production at the target; at low momenta the yield was also low, largely because of serious attenuation due to
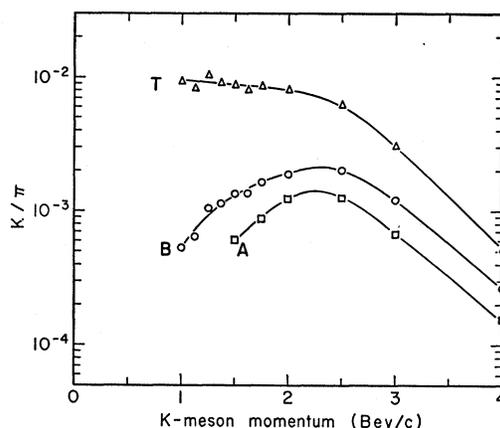
FIG. 5. The ratio of K mesons to π mesons actually recorded: Curves A and B refer, respectively, to mode A and mode B operation of the gas Čerenkov counters. Curve T shows the K/π ratio at the internal Bevatron target after the decay-in-flight corrections have been made.

decay in flight along the beam (about 100 ft long). Figure 5 shows the K/π ratio actually recorded for operation in modes A and B (see also Table I). The yield using mode A was poorer, since a K meson, in order to be counted efficiently in this mode, had to travel rather closely parallel to the axis of C_1 and C_2. Even then, fluctuations in photon number from the Čerenkov light could lead to further inefficiency. Also, the momentum width accepted was less in mode A than in mode B. The upper curve shows the K/π production ratio at the target, inferred by correcting the mode B curve for decay in flight of both π and K mesons.

At a few momenta, an estimate was made of how much the K/π ratio at the internal target depended on bevatron beam energy. Excitation curves obtained in this way are shown in Fig. 6. Fluctuations in the proton beam intensity and uncertainties in corrections for decay in flight were large, so that the absolute magnitude of the yield figures are probably correct only to about a factor of two.

III. TOTAL CROSS SECTIONS

In order to determine the total cross sections in hydrogen and deuterium, the hydrogen target was alternately filled and emptied several times, and the

TABLE I. Summary of the main characteristics of the secondary beam at different momenta.
Column 1 gives the momentum of the beam at production.

Momentum, p (Bev/c)	Momentum spread, $\Delta p/p$ (%)	Emission angle (rad)	Solid angle (msr)	π/p at target[a] (per % per msr)	K/p at target[a] (per % per msr)	Mean proton energy, $\bar{E}_p$ (Bev)
1	7.1	0.030	1.07	4.0×10^{-7}	1.8×10^{-9}	5.5
1.5	6.5	0.045	0.79	5.3×10^{-7}	2.9×10^{-9}	5.5
2.0	8.4	0.021	0.71	4.2×10^{-7}	3.0×10^{-9}	5.5
3.0	9.8	0.012	0.79	2.6×10^{-7}	0.65×10^{-9}	5.5
4.0	10.0	0.022	0.66	1.7×10^{-7}	0.11×10^{-9}	5.9

[a] Estimated correct within a factor of 2.

transmission measured in each case. The transmission counter T was a 9-in. diam circular scintillator mounted coaxially with the target and a few feet behind it. Its longitudinal position was varied depending on the momentum studied and was chosen always to minimize corrections to the final answer necessitated by Coulomb and diffraction scattering, beam divergence, inelastic processes, and decay in flight between target and counter. As a check on the effect of the forward-scattering correction, some measurements were made by using a 13-in.-square T counter placed further away. In a typical series of runs at a single momentum, a total of 3×10^5 K^- mesons was recorded by the counter T. The ratio of the transmission factors $(K+T)/K$ (full) and $(K+T)/K$ (empty) gave the transmission factor for the hydrogen or deuterium alone, and therefore the total cross section,

$$\sigma = (1/nL) \ln t,$$

where n = number of target nuclei per cm^3, L = length of target, and

$$t = \left(\frac{K+T}{K}\right)_{empty} \Big/ \left(\frac{K+T}{K}\right)_{full}.$$

The error in σ arising from the uncertainty in t is given by

$$\Delta\sigma = (1/nL)(\Delta t/t).$$

Under the pressure and temperature conditions at which the target was operated, the mass of hydrogen gas in the "empty" target was approx 0.4% of the liquid in the "full" target. Thus the atomic concentration n in the expression for σ refers to the difference in concentrations between liquid and gas.

Before the cross section could be obtained, several corrections had to be applied to the observed transmission factors. These were all small in this experiment; they are described below, and their magnitudes are listed in Table II.
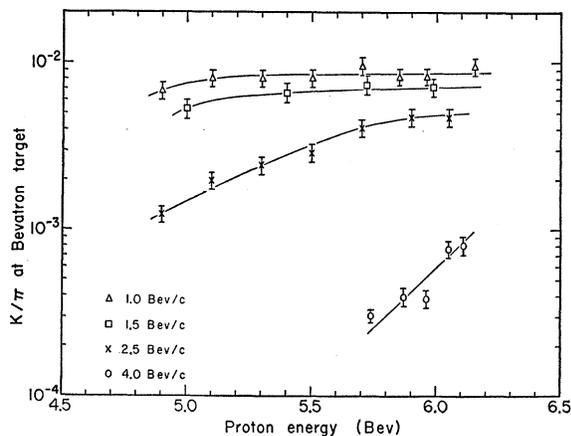
FIG. 6. K/π ratio at the internal target in the Bevatron as a function of incident proton energy. Values of p_K are shown on the different curves.

(a) *Change in decay rate.* The transmission factor for the empty target essentially measures attenuation due to decays in flight. When the target is filled, the loss in energy of the particles in the hydrogen modifies the decay rate slightly between the target and counter T.

(b) *Forward scattering.* K^- mesons interacting in the target can still be counted by T if they are scattered only through a small angle ($\lesssim 2$ deg). The value of the forward-scattering cross section is unknown over this energy region, except the measurement at 2 Bev/c described later (see Sec. V). From the optical theorem,[2] the imaginary part of the forward-scattering amplitude Im $f(0$ deg) is given by

$$\text{Im } f(0 \text{ deg}) = K\sigma_t/4\pi,$$

where σ_t is the total cross section and K the wave number. Thus

$$(d\sigma/d\Omega)(0 \text{ deg}) \geqslant [K\sigma_t/4\pi]^2.$$

In making these corrections, $f(0$ deg) was assumed purely imaginary. Thus, the correction is an underestimate if Re $f(0$ deg) is not negligible.

(c) *Rate sensitivity.* For a given incident flux, the counting rate in the T counter is not the same for both "target empty" and "target full" conditions, because of attenuation in the liquid hydrogen. So if equipment efficiency depends on the counting rate, the transmission factors "full" and "empty" are not directly comparable. All data on transmission factors from different runs at different energies were analyzed to see if there were any dependence on counting rate—the accidental rate was chosen as a useful variable with which to correlate the observed transmission factors. No evidence of correlation was found except for the deuterium "target empty" data, where there was a small but statistically significant effect. Accordingly, a correction was made as shown in Table II.

(d) *Light-particle contamination.* The effect of the K^- decay products counted in the T counter was estimated and found to be nearly independent of momentum and negligible in comparison with a, b, and c.

The above corrections were all small and applied to the cross sections in both hydrogen and deuterium.

In deducing the free-neutron cross section σ_n from the difference between σ_d and σ_p, a relatively larger correction had to be made for the screening of one nucleon by the other in the deuteron. This correction was made by using Glauber's formula,[3]

$$\sigma_n = \frac{\sigma_d - \sigma_p}{1 - (\sigma_p/4\pi)\langle 1/r_d^2\rangle},$$

where

$$\langle 1/r_d^2\rangle = (1/1.7)^2 \text{ f}^{-2}.$$

The errors quoted in Table II were compounded of

[2] E. Feenberg, Phys. Rev. **40**, 40 (1932).
[3] R. J. Glauber, Phys. Rev. **100**, 242 (1955).

TABLE II. Total cross sections for $K^- - p$, $K^- - d$, and $K^- - n$ interactions. The magnitudes of the included corrections are listed explicitly; see text for a discussion of how these have been calculated.

Momentum (Bev/c)		0.98	1.10	1.23	1.35	1.48	1.60	1.73	1.95	2.48	2.97	3.98
K^--proton												
σ_p(mb)		47.1±1.2	43.6±1.6	33.8±0.9	31.2±0.9	32.5±0.8	32.5±0.8	32.5±0.6	30.5±0.4	26.9±0.5	25.3±0.4	25.4±0.7
Correction	(a)	−2.4	−1.2	−1.0	−0.7	−0.8	−0.5	−0.5	−0.4	−0.2	−0.1	−0.1
included	(b)	+0.2	+0.4	+0.2	+0.3	+0.4	+0.4	+0.4	+0.4	+0.5	+0.5	+0.6
K^--deuteron												
σ_d(mb)		74.3±0.8		60.7±0.5		56.6±0.5		54.9±0.5	51.3±0.7	47.8±0.6	46.2±0.4	44.7±0.5
Correction	(a)	−1.7		−1.0		−0.7		−0.5	−0.3	−0.2	−0.1	−0.1
included	(b)	+0.7		+0.7		+0.9		+1.1	+1.3	+1.6	+1.8	+1.8
	(c)	+0		+0.2		+0.2		+0.3	+0.1	+0.5	+0.1	+0.2
K^--neutron												
σ_n(mb)		31.2±1.6		29.4±1.1		26.4±1.0		24.3±0.8	22.7±0.9	22.6±0.9	22.4±0.7	20.5±0.9
Correction included (Glauber)		+4.0		+2.5		+2.3		+1.9	+1.9	+1.7	+1.5	+1.2

three sources: (1) uncertainty in the corrections (a) to (d) listed above, (2) uncertainty in the atomic concentration n to be inserted in the cross-section formula, and (3) statistical errors.

The exact value of n was uncertain to the extent that the pressure and temperature of the gas in the "empty" target were not known exactly. The error in n is estimated to be about 0.3%. The statistical part of the error was computed internally from the total number of counts recorded, and externally by examining fluctuations of the subdivided data (in groups of about 20 000 counts each). In general, the group means exhibited a wider spread (between 1.1 and 1.3 times) than that calculated on the basis of purely random counting. Accordingly, the final statistical error was chosen to be 1.3 times that computed from the total number of counts at each momentum—this factor being the maximum ratio between externally and internally computed errors. It should be noted that the neutron cross sections may be further in error than the amount shown in Table II if the Glauber correction is not exact; no attempt was made to estimate the probable uncertainty due to this cause.

IV. CHARGE-EXCHANGE CROSS SECTION

A. Apparatus

For this part of the experiment the target was surrounded (except for a beam entrance hole) with the charged-particle and γ-ray detector A illustrated in Fig. 7. The wrap consisted of a layer of lead $\frac{1}{4}$ in. thick, outside of which 19 shaped plastic scintillation counters were fitted. The lead and scintillators were typically about 14 in. distant from the nearest point in the hydrogen target. Because of the high counting rate near the exit end of the target, a sandwich counter of two 13-in. scintillators with a $\frac{1}{2}$-in. layer of lead between them was placed to count with maximum efficiency the unscattered beam and γ rays emitted in the forward direction.

Assuming counter efficiency to be unity, measurement of the cross section for the reaction $K^- + p \rightarrow \bar{K}^0 + n$

involves counting only the fraction of anticoincidences in the counter wrap A per K^- meson entering the target. For, of the $\bar{K}^0$ mesons emitted in the charge exchange reaction, 50% decaying in the K_2^0 mode will, in a first approximation, pass through counter A before they decay and are recorded as anticoincidences. The remaining 50% decay through the short-lived K_1^0 mode close by the target and give rise to charged particles or γ rays which are detected in A. Any other elastic or inelastic interaction of K^- mesons with protons, insofar as these are known or can be surmised, also give rise to at least two charged particles or two γ rays. For example, when the secondary products of the K^- interaction are all neutral, the reactions may be summarized:

$$K^- + p \rightarrow \bar{K}^0 + n, \qquad \text{Charge exchange}$$

$$\left.
\begin{aligned}
&\rightarrow \bar{K}^0 + n + (1+x)\pi^0, \\
&\rightarrow \Lambda^0 \text{ or } \Sigma^0 + (1+x)\pi^0, \\
&\rightarrow \Xi^0 + K^0 + x\pi^0,
\end{aligned}
\right\}
\begin{aligned}
&\text{Inelastic, for } x=0, 1, 2, \\
&\quad \text{etc.,}
\end{aligned}$$
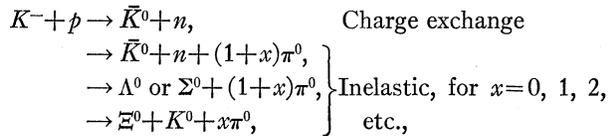
and it is clear that the short lifetime of both the hyperons and the π^0 meson ensures that all inelastic processes will give a count in A. In a first approximation, then, the ratio of counts $(K-A)/K$ is a direct measure of one-half the charge-exchange cross section σ_{ce}.

B. Results

The charge-exchange cross section was determined by means of the usual target-full, target-empty subtraction
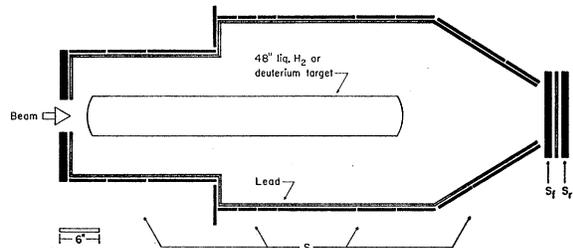
FIG. 7. An elevation view of the lead and scintillator wraps (A) surrounding the hydrogen target during the measurement of the charge-exchange cross section.

TABLE III. The cross section (in mb) for the "elastic" charge-exchange process $K^+ + p \rightarrow \bar{K}^0 + n$.

K^- momentum (Bev/c)	Target Hydrogen	Target Deuterium	Weighted mean
1	9.0 ± 1.9	12.9 ± 2.6	10.4 ± 1.7
1.5	3.2 ± 0.7	8.0 ± 1.9	3.8 ± 0.7
2.5	1.7 ± 0.6	1.9 ± 0.3	1.9 ± 0.3
4	5.4 ± 0.9	1.2 ± 0.6	2.5 ± 0.5

for both hydrogen and deuterium. Since only the proton in the deuteron is effective for charge exchange and a $K^- - n$ interaction leads to at least one charged product, the same cross section should be obtained from both experiments although the background events may be different. The results are presented in Table III.

The main sources of difficulty were the inefficiency of counter wrap A, especially for the detection of γ rays, and the smallness of the cross section σ_{ce} [for $\sigma_{ce} \approx 4$ mb, $(K-A)/K \approx 0.01$]. With the target empty, the $(K-A)/K$ rate varied monotonically from 2% at 1 Bev/c to 0.1% at 4 Bev/c, and was explicable entirely in terms of K mesons decaying in the $K_{\mu 2}$ mode, where the A counter sometimes failed to detect the single-charged decay product. From this, it was estimated that the efficiency for detecting just one charged particle in A was approx 95%. Thus the target-full minus target-empty difference was relatively smaller at the low momenta.

In deducing the cross section from the subtracted $(K-A)/K$ rates, corrections had to be applied as follows.

(a) *Beam attenuation*. The probability of charge exchange varied along the target because of beam attenuation in counter S_4 and in the target material. The attenuation cross section appropriate in this case was σ_a, the absorption cross section (approx $\frac{3}{4}\sigma_t$), because elastically scattered K^- mesons can still undergo charge exchange.

(b) *Decays in flight*. K^- mesons decaying in the $K_{\mu 2}$ mode within the "full" target might be recorded as anticoincidences because of counter inefficiencies. This correction could be reliably estimated from the target-empty rate, and was found to be 11% of σ_{ce} at 1 Bev/c and 3% at 4 Bev/c.

(c) *Non-charge-exchange events*. The inelastic reactions

$$K^- + p \rightarrow \Lambda^0 + \pi^0, \qquad K^- + p \rightarrow \Sigma^0 + \pi^0$$
$$\searrow \qquad\qquad\qquad \searrow$$
$$n + \pi^0, \qquad\qquad\qquad \Lambda^0 + \gamma$$
$$\searrow$$
$$n + \pi^0,$$
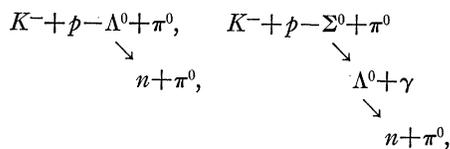
are the most likely of all non-charge-exchange reactions to lead to an anticoincidence in A because of inefficiency. On the basis of minimal estimates of a 90% efficiency in A for charged particles and 50% for γ rays, these

reactions had probabilities 0.06 and 0.03, respectively, of not being counted, while all other reactions had less than 0.01 probability of being missed. If the branching ratios found at 1.15 Bev/c for these modes[4] are taken as applicable over the whole momentum range, the correction to σ_{ce} is about 2.5%.

(d) *Loss of $\bar{K}^0$ mesons*. Some K_2^0 particles interacted in the inner wrap of lead, leading to charged particle production and so failed to register as an anticoincidence. This effect was estimated to be about 5%. Also, a small number of K_2^0 particles decay before escaping from the counter wrap and are also missed. This fraction was estimated to be about 3% at 1 Bev/c and about 1% at 4 Bev/c. On the other hand, particularly at high momentum, some K_1^0 particles failed to decay before passing through A and so were counted as a K_2^0 event. At the low momenta the correction was negligible, but at 4 Bev/c it amounted to 10%.

(e) *Glauber correction*. As with the total cross sections, a correction had to be made to the deuterium data to obtain the cross section on a free proton. Glauber's formula (see Sec. III) and the cross sections of Table II were used.

The quoted errors are those derived from the fluctuations of data taken in groups, which generally gave an answer about twice that derived from the total counting statistics alone. Since agreement between the hydrogen and deuterium data is not good, particularly at $p_K = 4$ Bev/c, it is possible that the quoted errors are underestimates, perhaps by a factor of about 2. It should be noted that the fundamental assumption in this method of measuring σ_{ce} is the validity of the K_1^0, K_2^0 particle-mixture hypothesis. One previous high-energy measurement of σ_{ce} has been reported, viz., $\sigma_{ce} = 7.8 \pm 1.1$ mb at $p_K = 1.15$ Bev/c.[4]

V. SMALL-ANGLE ELASTIC $K^- - p$ SCATTERING AT $p_K = 1.95$ Bev/c

A. Apparatus

Figure 8 shows the arrangement of the hodoscope used in studying the small-angle scattering of K^- mesons in hydrogen ($\theta_{lab} < 30$ deg). The first two sets of counters in the hodoscope, H_1 and H_2, consisted of 19 and 35 elements, respectively, each 8-in. high by 1 in. across. Knowledge of which elements in H_1 and H_2 the scattered particle crossed was sufficient to determine the angle of scattering to about 1 deg. Sets H_1 and H_2 were made up of $3 \times 8 \times \frac{1}{4}$-in. vertically mounted scintillators, each overlapping its two neighboring counters by 1 in. in horizontal projection, thus providing 1 in. spatial resolution (horizontally).

Were it not for the decay in flight of the K^- mesons,

---

[4] Luis W. Alvarez, in Proceedings of the Ninth Annual International Conference on High-Energy Nuclear Physics, Kiev, 1959 (unpublished); see also L. W. Alvarez, University of California Radiation Laboratory report UCRL-9354, August 11, 1960 (unpublished).

the two sets H_1 and H_2 would have been sufficient to determine the scattering distribution. However, the effect of decays in flight, both within and in the neighborhood of the hydrogen target, was to superimpose on the distribution of scattered K mesons a relatively more intense distribution of π mesons, μ mesons, and electrons with a variety of angles and momenta, most of which could simulate a small-angle $K^- - p$ scattering event. About 80% of these secondary decay-in-flight products could be rejected by using the magnetic field between H_1 and H_2 together with information from the third hodoscope set H_3. H_3 comprised fifteen $8 \times 3 \times \frac{1}{4}$-in. scintillators placed side by side, and had about the same angular resolution as sets H_1 and H_2. When a K^- meson was truly scattered by a proton in the target and when once the elements through which it passed in H_1 and H_2 became known, the position where it would strike H_3 was uniquely determined. If, however, a light particle arising from a decay in flight in the target passed through the same elements in H_1 and H_2, in about 80% of the cases it struck H_3 sufficiently far away from the appropriate place to allow it to be rejected unambiguously. The magnetic field was set at 14 kgauss, and the angle of bending for particles of momentum 1.95 Bev/c was about 12.5 deg.

The remaining 20% or so of decay-in-flight secondary particles which could not be rejected by magnetic sorting were those emitted forward in the c.m. system and having momenta close to that of the K mesons ($p_K = 1.95$ Bev/c). These, however, always had higher velocities than the scattered K mesons (thus $\beta_\pi = 0.998$ and $\beta_K = 0.97$, for $p = 1.95$ Bev/c), and were rejected by the anticoincidence Čerenkov counter C_3. The pressure of sulfur hexafluoride gas (250 psi) was chosen, so that the velocity threshold was above that for K mesons but below that for those light secondary particles which had almost the same magnetic rigidity. A particle with $\beta = 1$ produced a cone of Čerenkov light with $\theta = 10$ deg at this gas pressure.

Figures 9(a) and 9(b) show a plan and elevation view of the counter C_3. The sensitive volume of gas from

(a)

(b)

FIG. 9. (a) Plan of the sulfur hexafluoride gas Čerenkov counter C_3. (b) Elevation view of the sulfur hexafluoride gas Čerenkov counter C_3.

FIG. 8. Arrangement of the hodoscope magnet and gas Čerenkov counter C_3 used to measure the small-angle elastic $K^- - p$ scattering.

which Čerenkov radiation was detected efficiently was 48 in. wide, 10 in. high, and about 17 in. deep. Any Čerenkov light produced by particles crossing the device horizontally was focused by four 12-in.-square front-aluminized glass mirrors (28-in. radius of curvature) onto the four 5-in. Lucite windows shown. These Lucite windows served partly as field lenses and partly as light pipes, and directed the light onto the faces of the four RCA 7046 5-in. photomultipliers. The optical axes of the mirrors were tilted slightly from the perpendicular to the axis of the cylindrical pressure vessel in order to optimize the angular response of the counter for the horizontally divergent beam of particles arising in this experiment. Finally, a coincidence scintillation counter H_4, measuring 48×12 in., was placed behind the C_3 counter to ensure that only those particles were recorded which passed directly through the Čerenkov counter. The vertical apertures of H_1 and H_2 were delimited by requiring coincidences in two long scintillation counters, placed just behind them to avoid recording particles

that passed through H_1, H_2, and H_3, but had undergone scattering at either the top or bottom pole face of the magnet. These "vertical stop" counters were 4.5 in. high at H_1 and 6 in. high at H_2, and covered the full horizontal aperture of each. The vertical aperture of the magnet was $7\frac{3}{4}$ in.

The master signal corresponding to a true K-meson scattering was a coincidence of the type $K+H_4-C_3$, the signal K being as defined in Sec. II-B. Output signals from each of the counters in the hodoscope were put into coincidence with this master signal by means of separate diode coincidence units, and the outputs of these in turn were displayed and photographed in sequence on an oscilloscope. As a check on the electronic equipment, pulses K, H_4, and C_3 were also displayed on the trace.

The range of angles accepted was about 15 deg and was determined essentially by the horizontal aperture of the magnet. Absolute values of the scattering angles depended upon the orientation of the magnet with respect to beam direction. The angle between the face of the magnet and the beam is shown in Fig. 8 as 85 deg, but data were also recorded for settings at 80 and 90 deg. Running in the 80-deg position involved exactly the same procedure as in the 85-deg position. At the 90-deg setting, however, the main unscattered beam was allowed to pass through H_3 and C_3 and the following alterations were made. Where the main beam struck H_3, three adjacent counters were disconnected from the H_3 coincidence chain and then connected to form a separate transmission counter 8×9 in. called T^1. Directly behind the T^1 counter in the line of the main beam, one of the 12×12-in. scintillators normally forming part of H_4 was disconnected from the H_4 output and used to provide a separate output H_5. Thus the counting-rate ratio T^1/K measured attenuation due to the hydrogen target, the H counters, and the decay in flight, while the ratio H_5/K measured in addition the attenuation in the Čerenkov counter C_3. A total $K^- - p$ cross section at $p_K = 1.95$ Bev/c deduced from the T^1/K rates for full and empty targets was found to be in excellent agreement with that for the direct-transmission experiment.

TABLE IV. Summary of the data obtained in measuring small-angle $K^- - p$ elastic scattering for different experimental conditions.

Angle of magnet to beam (deg)	Target	Effective No. of incident K's	Approximate angular range (deg)	No. of scope sweeps	No. of apparent $K^- - p$ scatterings (after cutoff)
80	full	2.46×10⁶	8–27	14 967	1062
	empty	1.84×10⁶		11 173	107
85	full	1.44×10⁶	4–20	10 666	1111
	empty	1.39×10⁶		8711	250
90	full	0.76×10⁶	4–14	11 290	667
	empty	0.64×10⁶		9649	165

B. Results

Table IV summarizes data obtained for the various target and magnet conditions used in this part of the experiment. The effective numbers of incident K^- mesons given in column 3 were normalized to take account of the fraction of oscilloscope sweeps not studied (approx 17% lost or unreadable). Information from the traces scanned was recorded on IBM punched cards, and those events corresponding to the passage of a single particle through H_1, H_2, and H_3 were sorted into different angular categories defined by the H_1 and H_2 combinations, irrespective of which counter was triggered in H_3. For each of these categories the distribution of counters struck in H_3 was plotted and found in all cases to show a sharp peak at the position expected for a K meson of the right momentum. The target-empty data showed a similar peaking, indicating that the background events to be subtracted were also elastically scattered K^- mesons. By projecting back the orbits of these latter particles, it was found that almost all came from scattering in the aluminum end window of the target vacuum jacket and from the counters of H_1 close by the end of the target. The distribution in points of origin of every acceptable event was examined and there was no evidence of an appreciable contamination of events due to decays in flight where the Čerenkov counter C_3 had failed to reject the light secondary particle. For the selected $K^- - p$ scattering events, the subtraction ratio (full/empty) was about 10/1.

Table IV indicates that only a small fraction of the total sweeps scanned was accepted as due to genuine $K^- - p$ scatterings. Rejection of the balance of data was possible without ambiguity in almost all cases. Each rejected event was examined in detail to see how it could have happened. The three major causes of rejection were the following:

(a) *More than one counter element triggered in H_1 or H_2 or H_3 (approx 10%)*. Most of these events were due to inelastic interactions in which more than one energetic charged particle was produced. The number of cases in which just a single signal from H_1 and H_2, respectively, and a triple signal from H_3 were observed was of the right order to be explained in terms of τ decays in flight between H_2 and H_3.

(b) *Less than cutoff angle*. Because of intrinsic angular spread of the beam, and Coulomb scattering in the target and hodoscope counters, it was necessary to cut off traces accepted for data at some minimum angle. These effects were expected to become serious at $\theta_{lab} \sim 3$–4 deg, so a minimum accepted angle of $\theta = 5$ deg was adopted. At the 90-deg setting of the magnet, where very small scattering angles could be detected, about 25% of traces were rejected for this reason; at other settings the excluded fraction was about 7%.

(c) *Scattering of the main beam from the magnet*. The two vertical stop counters at H_1 and H_2, described in
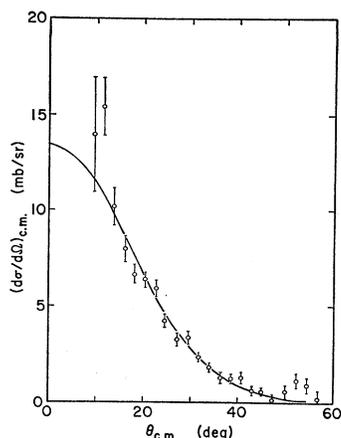
Fig. 10. Observed $K^- - p$ small-angle differential cross section per unit solid angle at 1.95 Bev/c. The solid curve corresponds to choosing $1 - a = C \exp[-(\rho^2/\langle\rho^2\rangle_{av})]$.

Sec. V-A, were efficient in rejecting events where the particle was scattered from either the top or bottom pole face of the magnet, but provided no protection against scattering from the side portions of the magnet yoke close to the median plane. For the 85-deg magnet setting, where the main beam grazed the side, and the 80-deg setting, where it strikes it completely, by far the greater number of traces (approx 69%) were caused by particles of the main beam scattering from the iron and parts of the coils and returning at an angle to pass through H_2 and H_3. The coordinates of the trajectory at H_1, H_2, and H_3 served to identify such events easily, and they were not confused with true $K^- - p$ scatterings.

Results obtained for the three magnet settings are shown in Fig. 10. The observed numbers were corrected for accidentals (about 5%), i.e., some of the events rejected for reason (a) above were due to genuine scattering events accompanied by a second accidental count, and also for a variation of decay-in-flight and attenuation losses with scattering angle. Errors on the points were largely determined by the counting statistics, but include also uncertainties in the corrections applied and uncertainties due to the selection of events of the right momentum from the distribution in counts across the H_3 set.

As a check for systematic errors, a subsidiary run was taken to measure $\pi^- - p$ diffraction scattering by tuning the Čerenkov counters to accept π mesons. The total number of incident π mesons used was 1.2×10^6, equally divided between target-full and target-empty runs. The results are shown in Fig. 11.

Since only a portion of the angular distribution was measured, it was not possible to make a phase-shift analysis. However, distribution in the angular range studied was largely dominated by the diffraction peak—as could be expected from the many inelastic channels available for K^--meson absorption—so that an optical-model approach was used to fit the data. Because of the

number of angular momentum states involved, it was found difficult to apply the method of Greider and Glassgold[5] in the absence of information at larger scattering angles. A "grey disk" type of analysis was found to give a satisfactory fit. Thus, if the fraction of the amplitude transmitted by the nucleon for a collision impact parameter ρ is denoted by a, then it was assumed that

$$1 - a = Cg(\rho),$$

where C is complex if there is real potential scattering. Then the differential cross section can be written

$$d\sigma/d\Omega = \sigma_0(1 - \tfrac{1}{2}q^2\langle\rho^2\rangle + \text{terms involving } \langle\rho^4\rangle, \langle\rho^6\rangle, \text{ etc.}),$$

where

$$\sigma_0 = \frac{d\sigma}{d\Omega}(0 \text{ deg}) = K^2|C|^2\left[\int g(\rho)\rho d\rho\right]^2,$$

$$q = \text{momentum transfer} = 2K\sin(\theta/2),$$

$$\langle\rho^n\rangle = \int \rho^n g(\rho)\rho d\rho.$$

In principle, it is possible to fit the data by a power series of this sort in q^2 and determine the moments of $g(\rho)$ and so the best shape which, in the spirit of this model, will explain the results. In practice, the data presented here require too many terms to allow the coefficients to be well determined. For a grey refracting disk (constant attenuation and constant phase shift within $\rho < R$), too sharp a minimum is predicted to fit the observed value. By tapering the edges, a more satisfactory fit can be obtained over fairly wide limits. A good fit is obtained by setting

$$g(\rho) = \exp(-\rho^2)/\langle\rho^2\rangle,$$
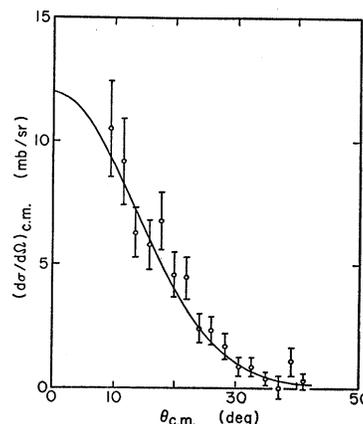
Fig. 11. Observed $\pi^- - p$ small-angle differential cross section per unit solid angle at 1.95 Bev/c. The solid curve corresponds to the same fitting function as for the $K^- - p$ scattering but with different values for C and $\langle\rho^2\rangle$.

[5] K.R. Greider and A. E. Glassgold, Ann. Phys. (N. Y.) 10, 100 (1960).

TABLE V. The parameters obtained by least-squares fits to the small-angle $K^- - p$ and $\pi^- - p$ scattering data, together with $P(\chi^2)$, the probability that the corresponding fit is a "good" one. Note that σ_0, D, and A all refer to the c.m. system.

	σ_0 (mb/sr)	Rms ρ (f)	$P(\chi^2)$ (%)	$\|D\|$ (f)	$A = \dfrac{K\sigma_T}{4\pi}$ (f)
$K^- - p$					
All points	13.5 ± 1.1	0.80 ± 0.03	8	$0.56_{-0.11}^{+0.10}$	1.02
Excluding two points	12.5 ± 1.3	0.78 ± 0.03	55	$0.45_{-0.17}^{+0.13}$	
$\pi^- - p$					
All points	11.9 ± 2.0	0.94 ± 0.09	76	$0.37_{-0.37}^{+0.21}$	1.025
Excluding two points	10.4 ± 1.9	0.79 ± 0.11	70	$0_{-0}^{+0.40}$	

which gives

$$d\sigma/d\Omega = \tfrac{1}{2}K^2|C|^2\langle\rho^2\rangle \exp(-\tfrac{1}{2}q^2\langle\rho^2\rangle) = \sigma_0 \exp(-\tfrac{1}{2}q^2\langle\rho^2\rangle).$$

Values of σ_0 and $\langle\rho^2\rangle^{\frac{1}{2}}$ obtained by the method of least squares are shown in Table V for the K^--meson data and for the subsidiary run with π^- mesons. The effect of omitting the two points at smallest angles is illustrated also. The errors on σ_0 and $\langle\rho^2\rangle$ are correlated (positively), and the quoted values are those corresponding to the χ^2 probability falling to half the best-fit value. These errors are about $1\frac{1}{2}$ times those given by the usual two-parameter least-squares fitting formula. Figure 10 shows the fitted curves. Since one is dealing here with a projected distribution, the spatial rms radius is obtained from $\langle\rho^2\rangle^{\frac{1}{2}}$ by multiplying by $(\frac{3}{2})^{\frac{1}{2}}$. For the π^- meson, then, this becomes 1.15 f, and for the K^- meson, 0.96 f. We write the forward scattering amplitude as $f(0$ deg$) = D + iA$, where $A = K\sigma_T/4\pi = 1.02$ f, from the σ_T data of Sec. III. Hence for K^- mesons, $|D| = 0.56 \pm 0.10$ f.

$|D|$ for the π^- meson is found to be $0.4_{-0.4}^{+0.2}$ f, which is to be compared with the value of 0.22 f obtained from a recent dispersion-relation analysis of available π^- experimental results.[6] The rms radial extension of the pion interaction found here 1.15 ± 0.11 f can be compared to the value of about 1 f resulting from several high-energy diffraction scattering experiments.

VI. DISCUSSION

A. Total Cross Sections

At momenta below a few hundred Mev/c the $K^- - p$ total cross section data are well fitted by a $1/v$ law, and have been investigated in terms of the S-wave zero-range approximation by Dalitz and Tuan,[7] and the effects of two pion exchange have been included by Ferrari et al.[8] The change in shape of the $K^- - p$ angular distributions between K^- momenta of 300 Mev/c and

400 Mev/c observed in bubble chamber experiments indicates a probable breakdown in the low-energy model.[4]

The data presented here (see Fig. 12) show that there is a rather abrupt change in slope of the cross-section curve at about $p_K = 1.25$ Bev/c. The structure in the cross section at this momentum is more evident if one looks at the imaginary part of the forward scattering amplitude given by the optical theorem (Fig. 13). The momentum width of the beam ($\approx \pm 3.5\%$) may be so large as to obscure any fine details of the structure in this region.

The K-neutron cross section σ_n has been measured at fewer energies and with less precision, but with increasing momentum it appears to fall steadily and shows no evidence of structure in the 1.25–2.0-Bev/c region. Since the $K^- - n$ system constitutes a pure $T = 1$ state and the $K^- - p$ system is a mixture of $T = 0$ and $T = 1$ states, the structure in the energy dependence is apparently associated only with the $T = 0$ K-nucleon state.

The structure in the $T = 0$ state may be attributed to one or more of a number of possible effects: (a) a resonance or resonances in the K-nucleon $T = 0$ state similar to those found in the pion-nucleon system at comparable energies, (b) rapid increase in the cascade particle production cross section above threshold, or (c) formation of isobaric states of two or three pions or of excited states of the nucleon or hyperon.[9]

For momenta higher than about 2 Bev/c the $T = 0$ cross section is larger than the $T = 1$ cross section by about 30%. Hence the theorem of Pomeranchuk,[10] which predicts equality of the cross sections in different isotopic spin states at high energies, is apparently not satisfied for the K^--nucleon system up to 4 Bev/c. That
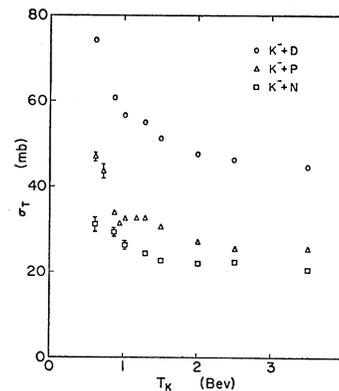
FIG. 12. The total cross sections for $K^- - d$, $K^- - p$, and $K^- - n$ interactions. Unless indicated, the vertical errors are smaller than the heights of the representative points.

[6] J. W. Cronin, Phys. Rev. 118, 824 (1960).
[7] R. H. Dalitz and S. F. Tuan, Ann. Phys. (N. Y.) 8, 100 (1959).
[8] F. Ferrari, G. Frye, and M. Pusterla, Phys. Rev. Letters 4, 615 (1960).

[9] M. Alston, L. Alvarez, P. Eberhard, W. Graziano, M. Good, H. Ticho, and S. Wojcicki, Phys. Rev. Letters 5, 520 (1960).
[10] I. Ia. Pomeranchuk, Zhur. Eksp. i Teoret. Fiz. 30, 423 (1956), [translation: Soviet Physics-JETP 3, 306 (1956)].
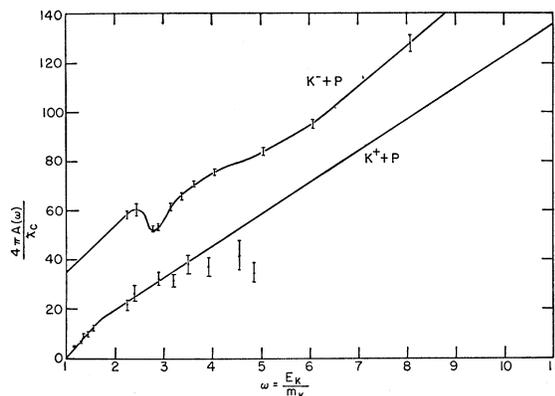
FIG. 13. The imaginary part of the forward-scattering amplitude for $K^- - p$ scattering as a function of energy. Points are calculated from the measured cross sections by using the optical theorem, and the interpolated curve is that used in the dispersion-relation calculations of Sec. VI.

the charge-exchange cross section does not vanish confirms this conclusion.

A final point in connection with the high-energy dependence of σ_p concerns the prediction of Pomeranchuk[11] that with certain plausible assumptions the cross sections of particle and antiparticle on the same target particle should tend asymptotically with energy to the same limit. As far as experimental measurements go, this tendency seems to be confirmed for the pion-nucleon interaction but not for K^+ and K^- at those energies. For K^- mesons, data from this experiment give a value $\sigma(K^-p) \approx 25$ mb, at high energies. The measurements by Burrowes et al., who found $\sigma(K^+p) \approx 13$ mb and decreasing at $p_K = 2.0$ Bev/c,[12] seem to indicate that in this region one is still far from observing asymptotic behavior. More recent data at higher energies and with larger errors, reported by von Dardel[13] up to 8 Bev/c, appear, however, to support the idea that $\sigma(K^+p)$ and $\sigma(K^-p)$ may approach a limit of approx 25 mb at high energies.

B. Differential Cross Section

The first feature to be noted in the results of the $K^- - p$ scattering experiment is the rather large value obtained for the rms value of the proton radius arising in the K^--meson interaction; this turns out to be only slightly less than that for the $\pi^- - p$ interaction. Secondly, the forward scattering cross section (13.6 ± 1.1 mb/sr) is significantly larger than that expected for pure diffraction scattering (10.4 mb/sr based on the total cross-section data of Sec. III) and implies the presence of a substantial amount of real scattering.

---

[11] I. Ia. Pomeranchuk, Zhur Eksp. i Teoret. Fiz. **34**, 725 (1958), [translation: Soviet Physics-JETP **34**, 499 (1958)].
[12] H. C. Burrowes, D. O. Caldwell, D. H. Frisch, D. A. Hill, D. M. Ritson, and R. A. Schluter, Phys. Rev. Letters **2**, 117 (1959).
[13] G. von Dardel, D. H. Frisch, D. Mermod, R. H. Milburn, P. A. Piroué, M. Vivargent, G. Weber, and K. Winter, Phys. Rev. Letters **5**, 333 (1960).

Dispersion relations for K-meson-nucleon scattering have been written by analogy with the π-nucleon dispersion relations.[14] These dispersion relations are most easily evaluated by computing the function $f(\omega)$ of the K-meson laboratory system energy, $\omega (\hbar = c = m_K = 1)$:

$$f(\omega) = \frac{1}{\pi} \int_1^\infty \frac{A_+(\omega')}{\omega' - \omega} d\omega' + \frac{1}{\pi} \int_{\omega_{\Lambda\pi}}^\infty \frac{A_-(\omega')}{\omega' + \omega} d\omega', \quad (1)$$

where $A_\pm(\omega)$ are the imaginary parts of the $K^\pm$-proton forward scattering amplitudes and $\omega_{\Lambda\pi}$ is the threshold for the reaction $K^- + p \to \Lambda + \pi$.

The dispersion relation then takes the form

$$D^+(\omega) = \left[\frac{2\langle pX \rangle_{av}}{(\omega + \bar\omega)} \right] + f(\omega),$$

where $\langle pX \rangle_{av}$ is the average contribution from the Λ and Σ poles, and $\bar\omega$ is the average energy of the two poles.

The function $A_\pm(\omega)$ is taken by using the optical theorem from the measured total cross sections. The values of $A_\pm(\omega)$ used in the experiment are shown in Fig. 13. In the unphysical region, the solution of Dalitz and Tuan was used,[7] assuming an attractive potential for the K^- interaction. Because there is a discrepancy in the K^+ data in the region of $\omega = 4$, a smooth curve was drawn between the points. Another smooth curve was drawn for the K^- data in the region $\omega = 1.13$ to $\omega = 3$, where no data exist.

Since the integrals in Eq. (1) must be cut off at $\omega_{max} = 16$ (the total cross sections are not known above this value), it is necessary to use a subtracted form of the dispersion relation that does not weight the high-energy data. One form is

$$D(\omega_1) - D(\omega_2). \quad (2)$$

The convergence of such a form has been considered by Amati et al.[15]

A second more convergent form by Karplus, Kerth,

TABLE VI. Values of the real part of the forward scattering amplitude and the values of the integrals at various ω's used in the dispersion calculation (in units where $\hbar = c = m_K = 1$).

$|\omega|$	D^+	D^-	$f(+\omega)$ ($\omega_{max} = 16$)	$f(-\omega)$ ($\omega_{max} = 16$)
1.00	-1.25 ± 0.14	$+4.5 \pm 0.5$	11.58	14.04
1.17	-1.24 ± 0.14	$+0.56 \pm 0.10$	13.52	13.20
1.285	-1.23 ± 0.14	$+0.40 \pm 0.10$	11.48	12.95
1.46	-1.2 ± 0.08	$\cdots$	11.43	12.64
1.92	-0.85 ± 0.08	$\cdots$	11.25	11.82
4.17	$\cdots$	$\pm(3.3 \pm 0.6)$	10.42	10.38

---

[14] R. H. Dalitz, in 1958 Annual International Conference on High-Energy Physics, CERN (CERN Scientific Information Service, Geneva, 1958), p. 191.
[15] D. Amati, M. Fierz, and V. Glaser, Phys. Rev. Letters **4**, 89 (1960).

and Kycia[16] is

$$\omega_0 D^+(\omega) - \tfrac{1}{2}(\omega_0 + \omega)D^+(\omega_0) - \tfrac{1}{2}(\omega_0 - \omega)D^-(\omega_0). \quad (3)$$

Experimental values of D are available at only a few values of ω. These are listed in Table VI along with values of $f(\omega)$ and $f(-\omega)$ for each.

From Table VI, various subtracted forms can be made up and the average pole term evaluated. Examples are given below for forms like Eq. (2):

$$D(-4.17)-D(-1.17), \quad \langle pX \rangle_{av} \begin{cases} =+3.6\pm0.5 \\ \quad \text{for } D^-(4.17)>0, \\ =-0.7\pm0.5 \\ \quad \text{for } D^-(4.17)<0, \end{cases}$$

$$D(1.92)-D(1.46), \quad \langle pX \rangle_{av} = -1.8\pm0.5,$$

$$D(-1.285)-D(1.285), \quad \langle pX \rangle_{av} = -0.05\pm0.3,$$

$$D(1.92)-D(1.00), \quad \langle pX \rangle_{av} = -1.0\pm0.2.$$

For forms like Eq. (3):

$$\omega=1.92, \quad \omega_0=1.00, \quad \langle pX \rangle_{av} = -0.35\pm0.4,$$

$$\omega=1.92, \quad \omega_0=1.285, \quad \langle pX \rangle_{av} = -1.5\pm0.5,$$

$$\omega=-4.17, \quad \omega_0=-1.285, \quad \langle pX \rangle_{av} \begin{cases} =+2.1\pm0.5 \\ \quad \text{for } D^-(4.17)>0, \\ =-0.5\pm0.5 \\ \quad \text{for } D^-(4.17)<0. \end{cases}$$

The significant point is that the value of the pole term from the various subtractions is different. Neither these values nor their quoted errors are statistically independent, since they all use the same total cross-section data and several use the same real forward scattering amplitudes. One explanation may be that the total cross section shows more structure than was assumed in the regions where no data exist. The region of $\omega=-1$ to

$\omega=-3$ is most important, since the greatest contribution to the integrals comes from this region.[16]

Both the total cross-section and forward-scattering data are still too few to allow a firm evaluation of the magnitude and sign of $\langle pX \rangle_{av}$. Internal consistency of the present calculations implies a value of $\langle pX \rangle_{av}$ in the region 0 to -1.0, but does not exclude small positive values; it furthermore strongly suggests that the sign of D^- at 1.95 Bev/c is negative. Thus the sign of the real part of the K^--proton potential at 1.95 Bev/c is opposite to that found at very low energies.[4]

C. Charge Exchange Cross Section

The "elastic" charge-exchange cross section falls from about 10 mb at 1 Bev/c to at most a few mb at 4 Bev/c.

[16] R. Karplus, L. T. Kerth, and T. Kycia, Phys. Rev. Letters 2, 510 (1959).

[16] *Note added in proof.* Recent measurements [O. Chamberlain, K. M. Crowe, D. Keefe, L. T. Kerth, A. Lemonick, Tin Maung, and T. F. Zipf, 1961; Alvarez 15-in. Bubble chamber group (unpublished, reported by M. Ferro-Luzzi at Strong Interactions Conference, Berkeley, December, 1960)] show that there is considerable structure in the K^-p total cross section in the range $\omega=1.4$ to $\omega=2.4$, and in fact there is a resonance at $p_K=1050$ Mev/c. Thus the smooth interpolation in this region assumed above is not correct; insertion of the new values improves the consistency of the $\langle pX \rangle_{av}$ results somewhat and does not alter materially the general conclusions above.